Journal of Molecular Liquids 309 (2020) 113065

Contents lists available at ScienceDirect

Journal of Molecular Liquids

journal homepage: www.elsevier.com/locate/molliq

# Effect of pH on the conformation of bovine serume albumin - gold bioconjugates

Bence Fehér [a,b], Jeppe Lyngsø [b], Boróka Bartók [a], Judith Mihály [c], Zoltán Varga [c], Róbert Mészáros [a,d], Jan Skov Pedersen [b], Attila Bóta [c,*], Imre Varga [a,d,**]

[a] Institute of Chemistry, ELTE, Pázmány Péter sétány 1/A, 1117 Budapest, Hungary
[b] Department of Chemistry and Interdisciplinary Nanoscience Center (iNANO), Aarhus University, Gustav Wieds Vej 14, 8000 Aarhus C, Denmark
[c] Research Centre for Natural Sciences, Institute oF Materials and Environmental Chemistry, Magyar tudósok körútja 2, 1117 Budapest, Hungary
[d] Department of Chemistry, University J. Selyeho, 945 01 Komárno, Slovakia

ARTICLE INFO

*Article history:*
Received 19 February 2020
Received in revised form 23 March 2020
Accepted 1 April 2020
Available online 17 April 2020

*Keywords:*
BSA
Gold
pH
Reversibility
SAXS

ABSTRACT

Biodegradable, biocompatible nanoparticles with tuneable fluorescence - due to their great potential in biology, medicine and sensor development - are widely studied nowadays. Recently it was shown that the complex red emitting spectroscopic feature of Bovine Serum Albumin - gold (BSA—Au) bioconjugates can be related to the versatility of conformational changes of the BSA protein. In our study, we performed a comprehensive study on the structural changes of the host BSA molecules by infrared spectroscopy (FTIR) and small-angle X-ray scattering (SAXS). Both methods revealed that the BSA structure is not reversible after a neutral - alkali - neutral pH cycle and this behaviour is more pronounced in the presence of the gold salt ($HAuCl_4$). The changes in the monitored secondary structural elements of BSA-($HAuCl_4$) system, with the fitted molecular shapes indicate that all steps in the synthesis route influence both the fine and the global structures of BSA and result in a complex structural prehistory dependent hindering of the total structural reversibility. A robust connection exists between the structural/conformational changes and the fluorescence behaviours.


## 1. Introduction

Fluorescent probes gained notable interest in the past few decades due to their widespread applications e.g. in the fields of sensing, molecular imaging, and labelling [1].One can find wide range of substances used as fluorescent dyes, which makes this method useful in numerous experimental settings and methodologies. At the same time the complexity of the potential applications creates an ever increasing demand for novel fluorophores with better biocompatibility, higher sensitivity and better spectral properties. Thus, it is not surprising that the recent discovery of a simple, one-pot synthesis of red fluorescent Bovine Serum Albumin / gold (BSA—Au) bioconjugates reported by Xie et al. [2] gained significant attention and triggered numerous investigations, which already lead to novel biosensors [3], and biomedical applications [4]. The BSA-Au bioconjugate has red fluorescence, which is especially desirable in biological applications due to the blue or green autofluorescence of tissue materials. The synthesis is a simple, one-pot method, which relies on the reaction of a commercially readily available protein, Bovine Serum Albumin (BSA) and hydrogen tetrachloroaurate ($HAuCl_4$) at a sufficiently alkaline pH (pH ~12).

BSA itself has autofluorescence in the blue region. In aqueous solution it can adopt five different conformations depending on the solution pH: expanded form (pH <2.7); fast form (pH = 2.7–4.3); normal form (pH = 4.3–8.0); basic form (pH = 8.0–10.0) and aged form (pH > 10.0) [5]. Using Nuclear Magnetic Resonance (NMR) measurements, BSA was found to be a dynamic protein that can affiliate its different conformations reversibly in the pH range from 2.51 to 10.21.

Despite its favourable properties and the large number of potential bioapplications, the physical nature of the BSA-Au bioconjugate is still not described unambiguously. Xie et al., stated that the fluorescent bioconjugate contains a gold nanocluster of 25 atoms, which is stabilized by BSA [2]. It has also been argued that the cluster contains gold atoms in the centre coated and stabilized with Au(I) cations [6]. There are also several studies suggesting that different pH levels used in the synthesis can result in different sizes of protein stabilized nanoclusters [7]. Later Dixon et al. found that the gold ions remain in the positively charged form during the reaction and that they form a red fluorescent complex with the aged form of the protein [8]. Investigations were also made to describe the fluorescent properties of the bioconjugate in different environments. Xie et al. found that despite the previously described reversible conformation changes of BSA with varying pH [5],

* Corresponding author.
** Correspondence to: I. Varga, Institute of Chemistry, ELTE, Pázmány Péter sétány 1/A, 1117 Budapest, Hungary
*E-mail addresses:* bota.attila@ttk.hu (A. Bóta), imo@chem.elte.hu (I. Varga).

https://doi.org/10.1016/j.molliq.2020.113065

the fluorescence of the BSA-Au bioconjugate remained unaffected in the pH range of 3–12 [2]. This may either mean that the fluorescence is not influenced by the conformational changes of the bioconjugate or the conformation of the protein does not change in the bioconjugate within the investigated pH range.

Dixon et al. on the other hand concluded that the fluorescence of the bioconjugate is linked to energy transfers among chromophores facilitated by the conformation of BSA at a specific pH. They suggested an equilibrium transition between blue and red emitting species with increasing pH, however, they did not test whether the formed red fluorescent bioconjugate goes through a reversible transition to the blue fluorescent form when the pH is decreased after the formation of the red fluorescent form [8]. Reports seem to agree that both extreme acidity and alkalinity results in conformational changes of the protein structure [9]. However, there is no evidence on reversibility of pH induced conformation changes in the bioconjugate and neither in the basic BSA molecules. The connection between the blue and red fluorescence forms and the different conformations seems to be a critical point of optical properties, therefore in the present work we extended the structural studies to a wide pH range occuring in the whole synthesis procedure.

## 2. Materials and methods

### 2.1. Materials

Bovine serum albumin (BSA, 96%) and $HAuCl_4\ 3H_2O$ (99.99%) were purchased from VWR and used as received. The pH of the solutions was adjusted by HCl (Sigma-Aldrich) and NaOH (Sigma-Aldrich). All solutions were prepared in ultrapure Milli-Q (total organic content = 4 ppb; resistivity ≥ 18 MΩ cm).

### 2.2. Sample preparation

A 5.0 w% BSA stock solution was prepared by dissolving BSA in Milli-Q water overnight then filtering the solution using a 0.2 μm sterile, nylon membrane filter. The filtered stock solution was kept at 5 °C in a fridge before further use typically for a day. 0.50 w%, pH = 7 (BSA-7) and pH = 12 (BSA-12) BSA solutions were prepared by ten times dilution of the BSA stock solution using Milli-Q water or a dilute NaOH solution, respectively. The concentration of the NaOH solution required to get pH = 12 BSA solution was determined by diluting several samples of the BSA stock solution with a series of dilute NaOH solutions and measuring the pH of the diluted 0.50 w% BSA solutions as a function of the NaOH concentration of the diluting solutions. The required NaOH concentration was determined by interpolation.

A 2.5 w% BSA/5.0 mM Au(III) stock solution was prepared by mixing the 5.0 w% BSA stock solution with 10.0 mM $HAuCl_4$ stock solution in 1:1 volume ratio at moderate stirring rate (600 rpm). When the prepared stock solution was diluted with Milli-Q water 5 times to get 0.5 w% BSA / 1.0 mM Au(III) solution, it had a pH = 4.2 (BSA/Au-4). To get pH = 7 (BSA/Au-7) and pH = 12 (BSA/Au-12) samples, the BSA/Au(III) stock solution was diluted by dilute NaOH solutions 5 times. The concentrations of the required NaOH solutions were determined in a similar manner as described above for BSA. Since according to Dixon et al. the pH = 12 BSA/Au(III) samples were heat treated at 37 °C for 2 h then stored at room temperature for two days to develop the red fluorescent bioconjugate, we followed the same protocol with half volume of the prepared 0.50 w%, pH = 7 and pH = 12 BSA (BSA-12HT) as well as with half volume of the prepared 0.5 w%, pH = 12 BSA / 1.0 mM Au(III) (BSA/Au-12HT) solutions. The other half of each solution was stored at room temperature without performing the 37 °C heat treatment.

The preparation of BSA and BSA/Au(III) samples with pH readjusted to pH = 7 from pH = 12 required a special care since the addition of concentrated HCl to the BSA solution resulted in the temporary aggregation of the protein sample. To avoid the loss of colloid stability of the protein molecules during the sample preparation first 0.75 w% BSA and 0.75 w% BSA / 1.5 mM Au(III) solutions were prepared. These samples were handled similarly to the 0.5 w% BSA and 0.5 w% BSA / 1.0 mM Au(III) samples but after the two days storage at room temperature their pH was readjusted to pH = 7 by diluting them with dilute HCl solutions. The final concentration of the samples were either 0.5 w% BSA (BSA—7Re) or 0.5 w% BSA / 1.0 mM Au(III) (BSA/Au-7Re), respectively. The concentration of the applied HCl solutions required to get pH = 7 were determined in a similar manner as the NaOH concentration to get pH = 12 BSA solutions (see above). The dilute HCl solution was added to the BSA solutions slowly from a Hamilton syringe under continuous stirring (600 rpm). It should also be noted that 0.75 w% BSA and 0.75 w% BSA / 1.5 mM Au(III) solutions were also diluted by pH = 12 NaOH solution to get 0.50 w%, pH = 12 BSA and 0.50 w%, pH = 12 BSA / 1.0 mM Au(III) solutions. The characteristic of these solutions were identical with the characteristic of the 0.50 w%, pH = 12 BSA and 0.50 w%, pH = 12 BSA / 1.0 mM Au(III) samples prepared directly from the stock solutions. (The sample names and sample histories are collected in Table. 1).

### 2.3. Sample characterization

*Fluorescent spectroscopy* measurements were performed with a Jasco Spectrofluorometer FP-8300. The fluorescent spectra were recorded using 360 nm excitation and 5 nm slit widths using a 3 × 3 mm quartz cuvette.

*Infrared spectroscopy* (ATR-FTIR) measurements were performed in attenuated total reflection (ATR) mode using a Varian 2000 (Scimitar Series) FTIR spectrometer (Varian Inc., US) equipped with a broadband MCT detector. As ATR unit, a single reflection diamond 'Golden Gate' ATR accessory was used (Specac Ltd., UK). 3 μL sample was pipetted onto the diamond ATR surface and dried under a gentle nitrogen stream. 64 scans were collected at a resolution of 2 $cm^{-1}$, keeping the sample under inert nitrogen atmosphere at all times. Spectral deconvolution was performed using the Grams/AI 7.02 (Thermo Galactic, US) software package. For curve fitting the number and peak positions of each band component were determined using the second derivative; band shapes were approximated by mixed Gaussian and Lorentzian functions until the minimum $\chi^2$ parameter was reached. The value of the Lorentzian contribution, the intensities and the bandwidth of each component were allowed to vary. After the fitting procedure, the relative contribution of a particular component was calculated from the integrated areas of the individual components.

*Small-angle X-Ray scattering* (SAXS) measurements were performed on an in-house instrument at Aarhus University, which is a Bruker AXS NanoStar with a Ga liquid metal jet source from Excillum [10] and home-built scatterless slits [11].The samples were equilibrated at 20 °C for 5 min prior to measurement. The acquisition time for each dataset was 600 s. Particle scattering is obtained from the data of the solution/mixture by subtracting the scattering of the matching solvent from

**Table 1**
The history of the 0.5 w% BSA and 0.5 w% BSA / 1.0 mM Au(III) samples prepared in this investigation. The details of the sample preparation are described in the text. All samples were measured four days after the stock solutions were diluted.

| Sample | Sample history |
|---|---|
| BSA-7 | Set pH = 7: 4 days at room temperature (RT) |
| BSA-12 | Set pH = 12: 4 days RT |
| BSA-12HT | Set pH = 12: 2 h 37 °C, 4 days RT |
| BSA-7Re | Set pH = 12: 2 h 37 °C, 2 days RT / Set pH = 7: 2 days RT |
| BSA/Au-4 | Set pH = 4: 4 days RT |
| BSA/Au-7 | Set pH = 7: 4 days RT |
| BSA/Au-12 | Set pH = 12: 4 days RT |
| BSA/Au-12HT | Set pH = 12: 2 h 37 °C, 4 days RT |
| BSA/Au-7Re | Set pH = 12: 2 h 37 °C, 2 days RT / Set pH = 7: 2 days RT |

that of the sample. The initial data treatment was done using the SUPERSAXS program package (Oliveira, C.L.P. and Pedersen, J.S., unpublished) using Milli-Q water as a standard for absolute scale calibration. The intensity of the scattered X-rays is given as a function of the modulus of the scattering vector:

$$q = \frac{4\pi}{\lambda} sin\theta \quad (1)$$

where λ is the wavelength of the incident radiation and $2\theta$ is the scattering angle. For samples containing particles, the total measured intensity can be written as the contribution of the normalized form factor $P(q)$, which is determined by the size and the shape of the particles, and the structure factor $S(q)$, which arises from interference between the X-rays scattered by different particles in the sample. The scattered intensity is expressed as:

$$I(q) = \frac{N}{V} P(q) S(q) \quad (2)$$

where $N/V$ is the number density of particles.

To obtain the structure of the native BSA at pH = 7 an in house program 'wlsqsymxv5XL' [12] was used, however to obtain the structure of the BSA-Au system under different conditions, rigid-body refinement was performed using SASREF [13] after splitting the structure into 4 domains. SASREF performs structural modelling of the BSA using appropriately connected domains of the protein with known atomic structures obtained from the Protein Data Bank (PDB entry: 4F5S [14]). With both programs 10 runs were performed for each dataset and the resulted structures were analyzed by DAMAVER [15]. Damsel was used to compare the datasets and for the alignment Damsup was used. The structure with the less normalized spatial discrepancy (NSD) was chosen as the representative structure.

## 3. Results and discussion

To address the reversibility of the pH variation induced conformational changes of BSA both in the absence and in the presence of gold ions, we investigated the effect of pH changes on both BSA and BSA-Au samples. First BSA (5.0 w%) and BSA-Au (2.5 w% / 5 mM HAuCl4) stock solutions were prepared in Milli-Q water at room temperature. The BSA stock solution was diluted 10-fold by either Milli-Q water or a dilute NaOH solution to get 0.5 w% pH = 7 (BSA-7) and pH = 12 solutions (BSA-12), respectively. The BSA-Au stock solution was also diluted 5-fold by two different concentration NaOH solutions to get 0.5 w% / 1 mM $HAuCl_4$ pH = 7 (BSA/Au-7) and pH = 12 (BSA/Au-12) solutions. Since previous investigations showed [8] that the red fluorescence of BSA-Au conjugates develop in two days after a 2-h heat treatment performed after setting the pH to 12, half of all pH = 12 solutions were heat treated at 37 °C for 2 h (BSA-12 HT and BSA/Au-12HT) then all solutions were stored at room temperature for two days. Finally the pH of a set of the pH = 12 samples was adjusted to pH = 7 by dilute HCl solutions (BSA-7Re and BSA/Au-7Re) and were stored for an additional two days at room temperature (for details see the Experimental section). Samples from each stage of the pH cycle were measured by IR, SAXS and fluorescent measurements 4 days after the initial stock solutions were prepared to monitor the conformational and structural changes of the protein as well as the variation of its fluorescent characteristics.

In Fig. 1 the fluorescent emission spectra of BSA and BSA-Au samples are shown as a function of pH cycling. As it is revealed in panel-A BSA shows weak blue fluorescence under λ=360 nm excitation (BSA-7). Interestingly, increasing the pH from 7 to 12 (BSA-12) has only a small effect on the fluorescence of the protein. Further, heat treating the pH = 12 sample (BSA-12HT) for 2 h at 37 °C practically leaves the fluorescence of the protein unaffected. At the same time when the pH is decreased from 12 to 7 again (BSA—7Re), the fluorescence increases further significantly (~50%), instead of decreasing to its original lower value. This hints that the protein structure/conformation must preserve permanent changes due to the pH cycling from 7 to 12 then to 7 again.

In Fig. 1B the fluorescence spectra of the BSA-Au solutions are shown. In agreement with previous results the pH = 7 sample (BSA/Au-7) showed only blue fluorescence. At the same time the intensity of the fluorescence is much larger in the presence of gold ions implying that protein/gold ion interaction occurs already in this case. When the pH of the BSA-Au solution is increased to pH = 12 (BSA/Au-12) the red fluorescence appears as it is described in the literature. At the same time it is interesting to note that after four days of room temperature storing the effect of the two hours heat treatment at 37 °C (BSA/Au/12HT) is practically negligible on the sample fluorescence. Finally, when the pH of the BSA-Au solution was set back to pH = 7 (BSA/Au-7Re), the fluorescent characteristics of the samples changed significantly. Contrary to pure BSA, in this case the blue fluorescent peak decreased somewhat, however it remained much larger than its original value at pH = 7. At the same time the red fluorescent peak increased in a large extent (~250%). This observation strongly implies that during the pH cycle the structural and conformational states cannot be reverted by returning to the original pH.

To get an insight what kind of conformational and structural changes take place during the pH cycle in the protein we performed IR and SAXS measurements. Regarding the IR analysis, we focused on the two major amide bands of the protein infrared spectra (Figs. 2, 3). The amide I band (between 1700 and 1600 $cm^{-1}$) is mainly related to the C═O stretching vibration (70–85%) and can be directly correlated to the peptide backbone conformation (each type of secondary structure has slightly different C═O stretching). At the same time the amide II band is related to the N—H bending vibration (40–60%) and the C—N stretching vibration (18–40%) [16] [17], and it is also sensitive to conformational changes. The results of IR analysis are collected in Table. 2.

When the pH of the BSA solution is increased to pH = 12 (BSA-12), significant changes can be observed in the amide I and amide II band envelopes (Fig. 2A, B) compared to the pH = 7 sample (BSA-7). The band components show an increase in turn and sheet-like structures at the

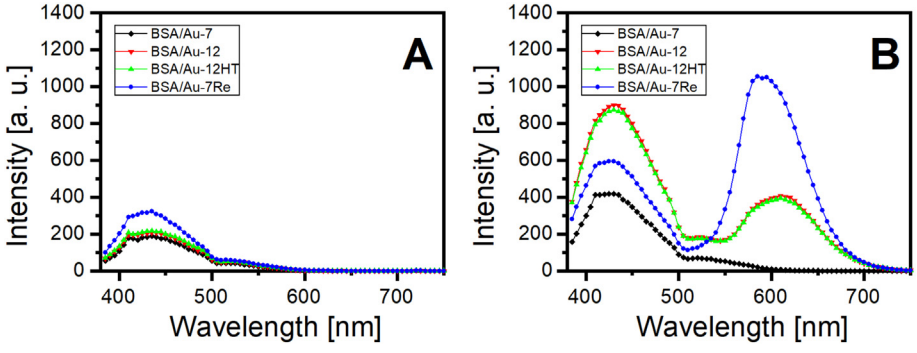


**Fig. 1.** The fluorescent spectra ($\lambda_{EX}$=360 nm) of A: 0.5 w% BSA and B: 0.5 w% BSA - 1 mM Au(III) samples.

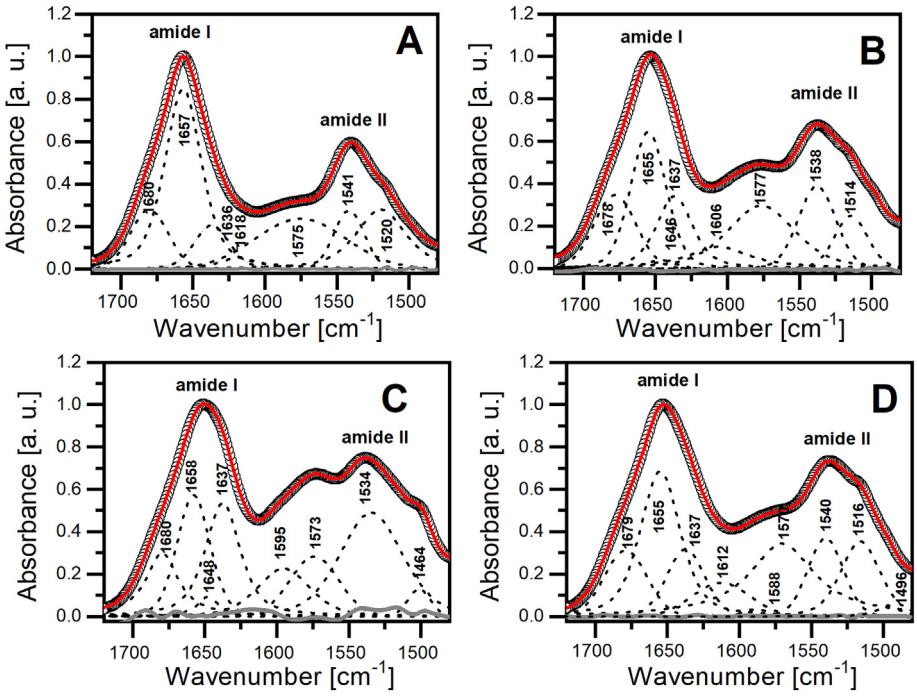


**Fig. 2.** The deconvoluted amide I and amide II bands of BSA at different pH and treatment conditions: A: BSA-7; B: BSA-12; C: BSA-12HT; D: BSA—7Re. For details of sample preparation see Table 1. Symbols represent the original data point; solid red line is the fitted curve; dashed lines denote component bands; grey solid line is the fitting residual.

expense of helical conformations. The peak position of the latter is also shifted towards lower wavenumber (from 1657 $cm^{-1}$ to 1655 $cm^{-1}$), which suggests enhanced H-bonding. The band component around 1643 $cm^{-1}$, witnessed in the spectrum of BSA at pH = 12 can be assigned to unordered, random coil structure [16] [18]. Simultaneously, the shape of amide II band is also altered. The differences in intensity ratios of amide I/amide II bands can be related to difference in protein tertiary structure [19].

Indeed, the relative intensity of the amide II band around 1538 $cm^{-1}$ (corresponding to N—H bending and C—N stretching of peptide bonds) is increased, suggesting an alteration in tertiary structure of the protein. We have to note, however, that since the IR spectroscopy is highly sensitive to COOH and $COO^-$ groups, changes in side chain protonation of the proteins can be also followed. The increased band at 1577 $cm^{-1}$ and the new band at 1606 $cm^{-1}$ can be assigned to asymmetric stretching of $COO^-$ probably from amino acid side chains and to the Tyr-$O^-$ stretching, respectively. It seems plausible, that at pH = 12 the BSA backbone became more extended, with loose unordered parts allowing charged side chains to be accessible. Heat treating (at 37 °C for 2 h) (BSA-12HT) further enhance these changes. Both the $\beta$-sheet/helix ratio and the intensity of charged and accessible side chains are further increased. After readjustment of the pH to neutral (BSA—7Re), the protein structure seems to approach the initial conformation, however the initial stage is not recovered. Changes in both secondary and tertiary structure were preserved as indicated by the extended ratio of sheet-like conformation and by the shape and intensity of the amide II band envelope similar for protein spectrum recorded at pH = 12.

Similar IR spectroscopy based inspection on BSA structure was performed in the presence of $HAuCl_4$ (Fig. 3). The addition of the required amount of $HAuCl_4$ salt resulted in a significant decrease in the pH value of the system, which was accompanied with a small alteration in secondary and tertiary structure of BSA (BSA/Au-4). The amount of sheet-like structures increased at the expense of helical conformers, and the relative intensity of amide II band around 1540 $cm^{-1}$ was also increased. It is interesting to observe, that turning to neutral pH (BSA/Au-7) the BSA does not restore its initial structure (BSA-7). Based on the IR spectrum the relative intensity of bands at 1637 and 1612 $cm^{-1}$ of sheet-like conformers are increased, the latter being characteristic of intermolecular $\beta$-sheet from aggregates [17] [20]. When the pH of the acidic BSA-Au samples were increased to 12 in the presence of $HAuCl_4$ (BSA/Au-12), the $\alpha$-helix to $\beta$-sheet ratio of the BSA is more significant decreased. Both at neutral and basic pH, the component bands of amino acid side chains (similar to that of BSA at pH = 12) are more pronounced, suggesting that addition of NaOH provoke a looser, more accessible structure of protein. After heat treatment (37 °C for 2 h) (BSA/Au-12HT) the band intensity related to $COO^-$ from side chains are further enhanced. After readjustment to neutral pH (BSA/Au-7Re) the extended amount of sheet-like structure is preserved, resulting in a helical to sheet conformation ratio slightly lower (2.3 in Table 2) than for pure BSA after pH and heat treatment cycle (2.6 in Table 2) and relatively lower than for BSA-Au system at pH = 7 (3.4 in Table 2). After the pH cycle the incomplete recovery of BSA-Au conformation is expressed by the comparison of the beginning and final spectra (Fig. 3F). Besides the $COO^-$ asymmetric stretching at 1571 $cm^{-1}$, the band corresponding to Tyr-OH at 1516 $cm^{-1}$ is dominating the amide II band envelop. It seems plausible that the charged Tyr-$O^-$ groups formed after NaOH addition are protonated by lowering the pH.

The SAXS data of BSA dissolved in water and adjusted to different pH values are shown in Fig. 4. The Kratky plots corresponding to these states are also presented in the right panels of Fig. 4 to highlight the effects of the different pH milieus on the protein conformations. The scattering curve of the neutral BSA system (BSA-7) (1A in Fig. 4) does not correspond to the ideal dilute solution scattering from randomly oriented monodisperse particles. In the low-q range, a wide minima can be observed, which is a consequence of the present structure factor effects due to the relatively high BSA concentration and the absence of salt. These conditions were required for an effective sample preparation process. The Kratky-plot of BSA (BSA-7) (1B in Fig. 4) indicates the existence of a multidomain structure with flexible parts (partially flexible subdomains). In alkali milieu (BSA-12) the conformation of BSA changed drastically, as the significantly altered SAXS curve suggests (2B, 3B in Fig. 4). In the high-q range, the slope of the curve is smaller than that of the globular and compact BSA, indicating the chain-like polymeric behaviour of the high pH BSA conformation. The severe

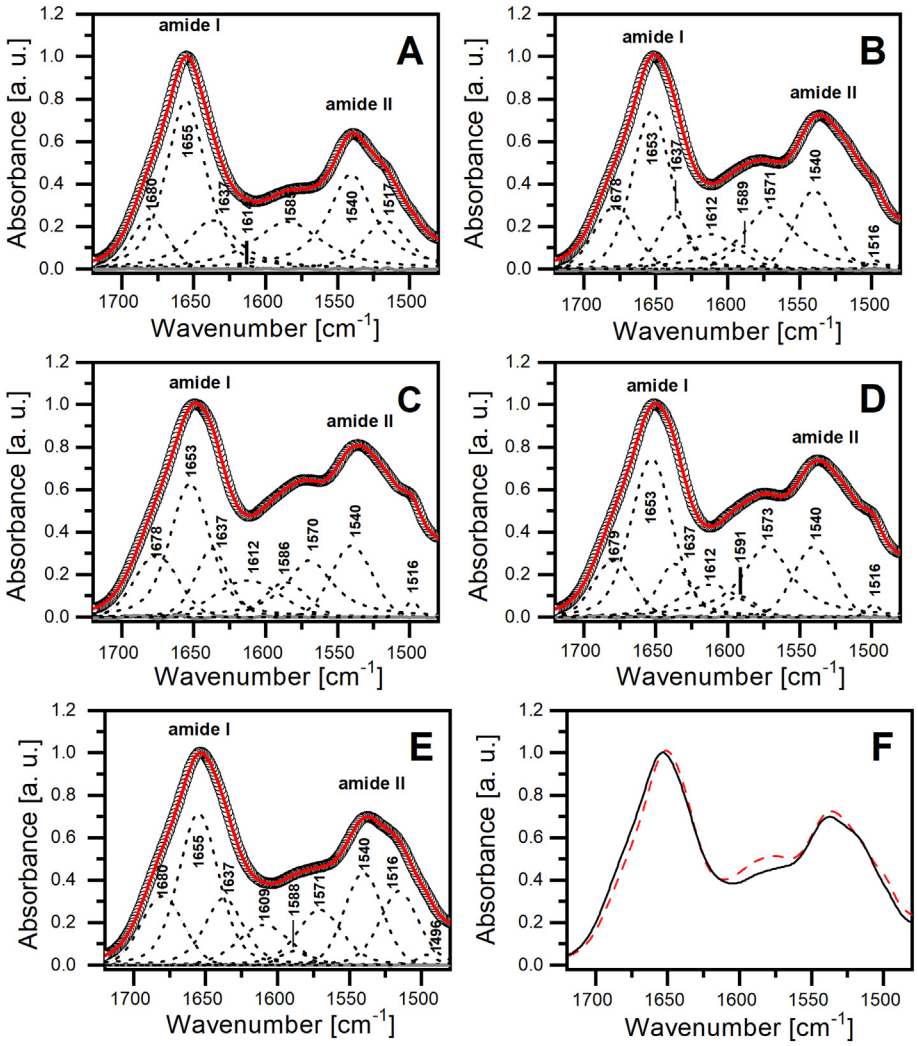


**Fig. 3.** The deconvoluted amide I and amide II bands of BSA-$HAuCl_4$ system at different pH and treatment conditions: A: BSA/Au-4; B: BSA/Au-7; C: BSA/Au-12; D: BSA/Au-12HT; E: BSA/Au-7Re; F: comparison of BSA-$HAuCl_4$ systems at pH = 7 (BSA/Au-7: red spectrum and BSA/Au-7Re: black spectrum. For details of sample preparation see Table 1. Symbols represent the original data point; solid red line is the fitted curve; dashed lines denote component bands; grey solid line is the fitting residual.

change in the slope of the scattering curve is likewise observed in the Kratky plot, as the $I(q)\cdot q^2$ values diverge as a function of q (2B in Fig. 4). At the same time, the typical main peak in this representation, indicative of globular folding, is strongly reduced suggesting the unfolding of the protein to a large degree in full agreement with the spectroscopic findings. Contradictory to the IR measurements, the the heat treatment of the BSA sample (BSA-12HT) does not induce any observable conformational changes in BSA, as the SAXS data and the corresponding Kratky plots exhibit identical profiles (Fig. 4 2A-B and 3A-B). Surprisingly, after adjusting the pH value back to neutral (BSA—7Re), the scattering curves now differ from the original curves (BSA-7), indicating that the unfolded structure does not fold back to the starting state and the pH cycling is therefore not reversible (4A in Fig. 4). In the low-q interval, between $10^{-2}$ and $5{\cdot}10^{-2}$Å$^{-1}$, which previously showed significant structure factor effects, the unperturbed characteristic form factor scattering curve of a globular structure is now visible. This phenomenon can be explained by the increased ionic strength achieved during the steps of the pH adjustment process where alkali (NaOH) and

**Table 2**
Estimated secondary structure of BSA systems based on deconvolution of amide I IR band.

| | α-Helix % | β-sheets % | Intermol. β-sheets % | β-turns % | Random coil % | Helix/sheets ratio |
|---|---|---|---|---|---|---|
| BSA-7 | 63 | 13 | 5 | 18 | – | 4.7 |
| BSA-12 | 43 | 27 | – | 27 | 3 | 1.6 |
| BSA-12HT | 34 | 39 | – | 23 | 5 | 0.9 |
| BSA-7RE | 48 | 19 | 14 | 20 | – | 2.6 |
| BSA/Au-4 | 51 | 13 | 11 | 25 | – | 2.5 |
| BSA/Au-7 | 51 | 15 | 15 | 19 | – | 3.4 |
| BSA/Au-12 | 45 | 18 | 17 | 19 | – | 2.5 |
| BSA/Au-12HT | 54 | 15 | 14 | 17 | – | 3.7 |
| BSA/Au7RE | 50 | 19 | 10 | 21 | – | 2.3 |

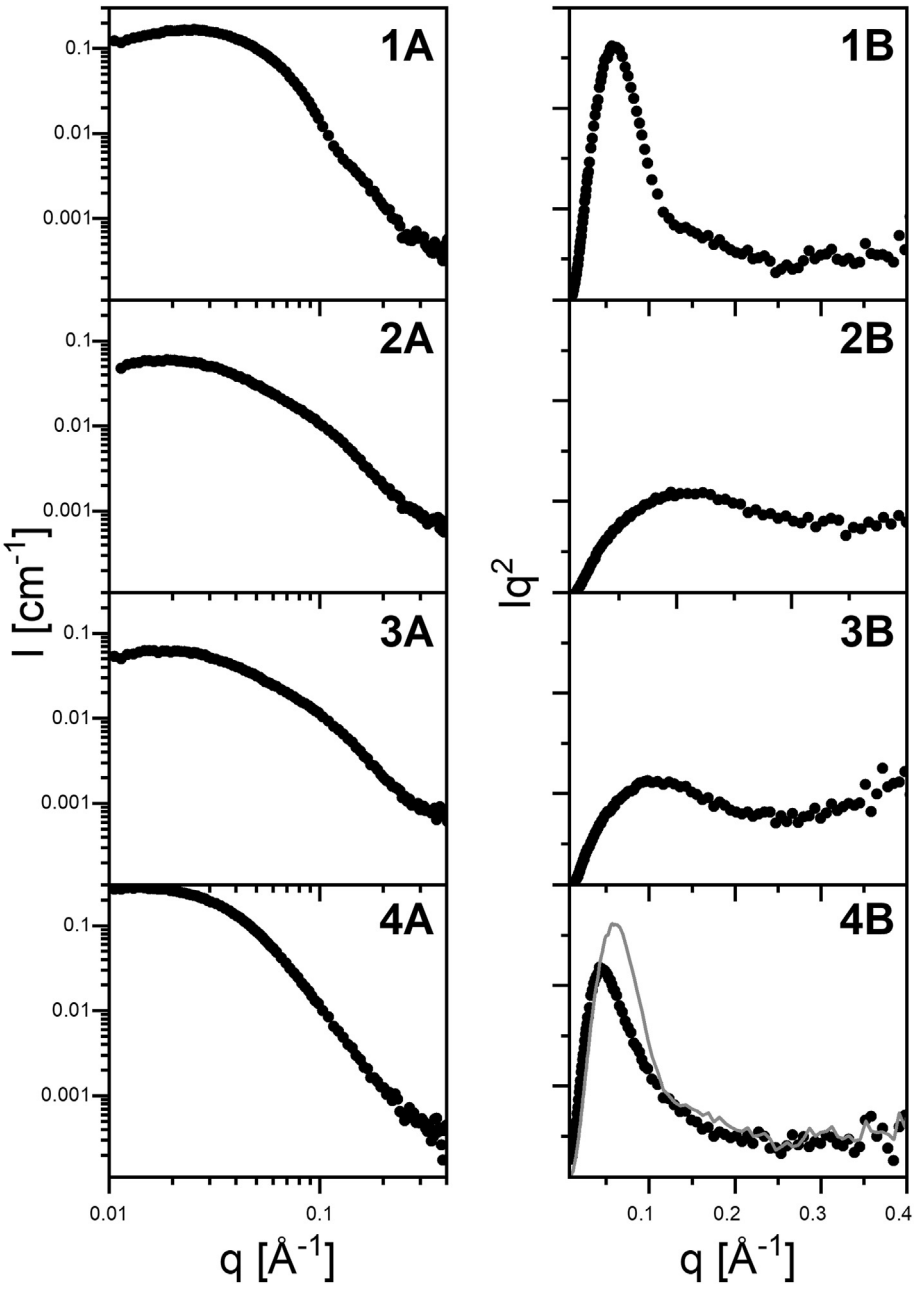


**Fig. 4.** SAXS curves of BSA (A) and the corresponding Kratky plots (B). 1A, 1B: BSA-7, 2A, 2B: BSA-12, 3A, 3B: BSA-12HT, 4A, 4B: BSA—7Re. The red line in panel 4B shows the Kratky plot of pH = 7 (BSA-7) sample in order to emphasize the irreversibility of the structure.

acidic (HCl) substances were added. The difference between the Kratky plots (4B in Fig. 4) indicates a change in the multidomain structure that was also witnessed by IR spectroscopy (Fig. 2).

The presence of $HAuCl_4$ induced significant changes in the BSA conformation at all pH values as it can be observed in Fig. 5. After adding gold salt to BSA (BSA/Au-4), the SAXS curve shows no structure factor, presumably due to the surface effect of $HAuCl_4$ (1A in Fig. 5). The domain structure, however, is also altered at pH = 7 (BSA/Au-7), as it can be seen in the Kratky representation (1B in Fig. 5). The characteristic peak is significantly broadened relative to that of BSA without gold salt (1B in Fig. 4), indicating the existence of a dominantly globular but perturbed state with flexible subdomains. When the pH value is adjusted to 12 (BSA/Au-12), the scattering curve again indicates a chain-like behaviour, as was observed in the absence of $HAuCl_4$, however, the extent of unfolding seems to be greater in the presence of gold salt (3A in Fig. 5). Indeed, the Kratky plot exhibits an extended section with a positive slope in the range of high-q values (3B in Fig. 5). In presence of gold salt, the SAXS measurements do not indicate structural changes due to the heat treatment of the sample (BSA/Au-12HT)(4A and 4B in Fig. 5). At the same time, similarly to the $HAuCl_4$-free cases, the effect of the heat treatment was observed by spectroscopy, indicating that these changes do not influence the global, SAXS revealable, structure significantly. After readjusting to neutral pH (BSA/Au-7Re), the conformational change of BSA is significant, and it differs drastically from that of the gold salt-free state (BSA-7). The changes are well illustrated by the Kratky plot (5B in Fig. 5). The peak, characteristic for globular domains, is partly recovered, but the remaining part of the curve diverges, indicating clearly that in this altered conformational state folded and flexible domains coexist.

To reveal the structure at the different stages of the protein unfolding induced by the pH variation and the addition of the gold ions, we performed rigid-body refinement with SASREF on the BSA-Au

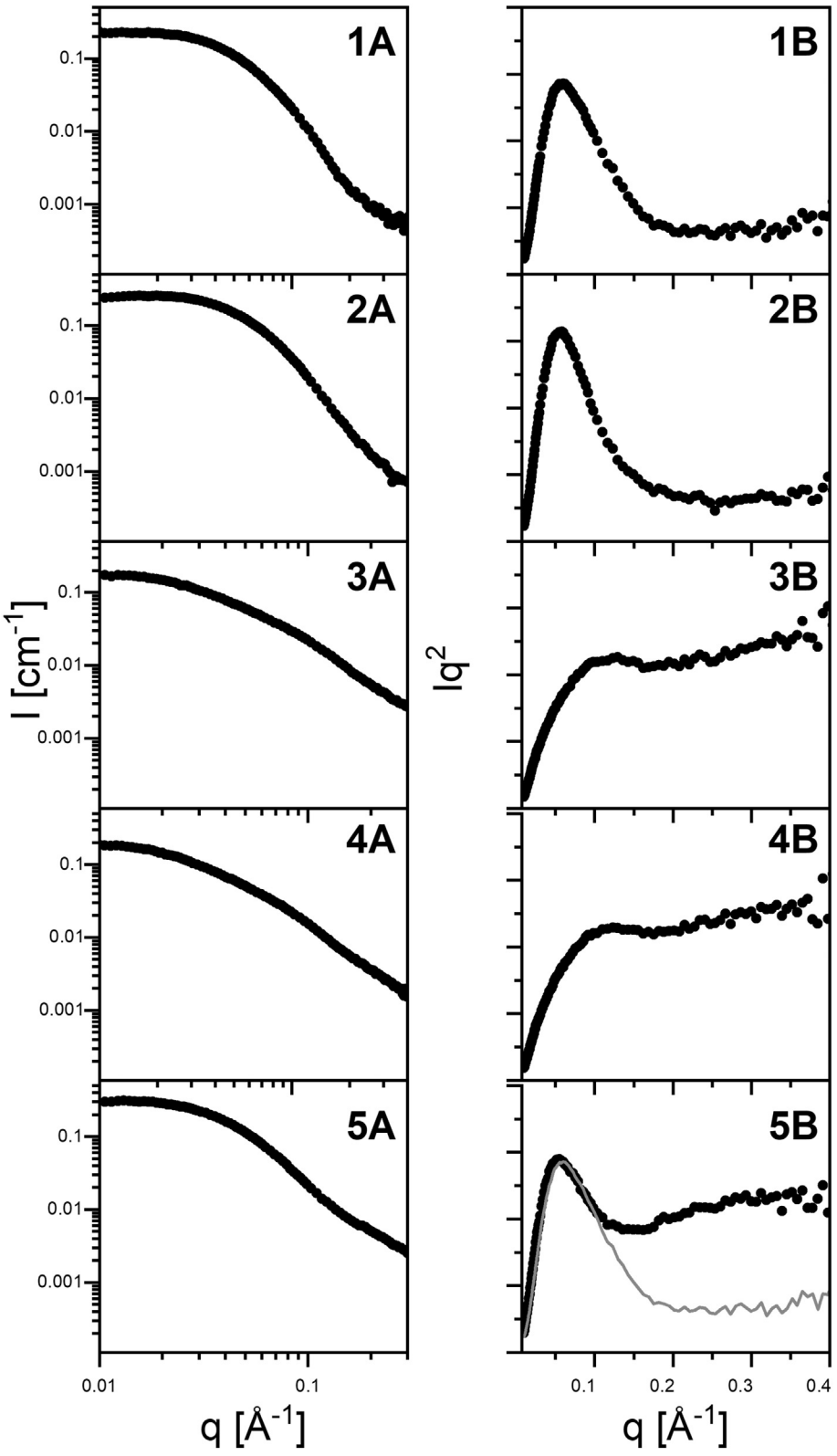


**Fig. 5.** SAXS curves of BSA-$HAuCl_4$ systems (A) and the corresponding Kratky plots (B). 1A, 1B: BSA/Au-4, 2A, 2B: BSA/Au-7, 3A, 3B: BSA/Au-12, 4A, 4B: BSA/Au-12HT, 5A, 5B: BSA/Au-7Re. The red line in panel 5B shows the Kratky plot of pH = 7 sample (BSA/Au-7) in order to emphasize the irreversibility of the structure.

systems. The native BSA structure was cut into four linked domains (marked by different colors Fig. 6: domain I: orange, domain II: green, domain III: blue, and domain IV: yellow). Since the IR measurements indicate a 10% difference in the $\alpha$-helical content of the heat treated and the not heat treated BSA samples, while the heat treatment has no effect on the scattering curve, we concluded that we can neglect the changes in the secondary structure when modelling the globular structure. Thus, during the optimization, the $\alpha$-helix, $\beta$-sheet, and random coil content was kept constant. Increasing the pH value to 12, the SAXS data can not longer be fitted with the four domains by simple rigid

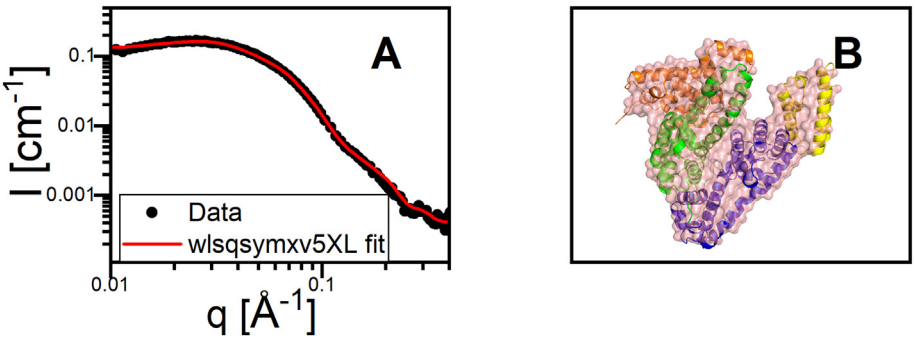


**Fig. 6.** A: Representative SAXS curve of BSA-7 fitted by wlsqsymxv5XL, B: the obtained structure.

rigid-body refinement modelling, which suggests that the behaviour of the BSA is more polymer-like under these conditions as expected. However, we have to emphasize, that if the protein, in the extreme case, was fully unfolded the SAXS data could be fitted with a Debye chain model [21] which is not the case. This fact allows us to conclude that the structure under these severe conditions is more likely to consist of $\alpha$-helix segments connected by random coil sections.

The native BSA (BSA-7) was fitted by the in-house program called 'wlsqsymxv5XL' to include the structure factor (scattering curve, fit, and corresponding protein structure is shown in Fig. 6). When gold is added to the BSA, the pH drops to 4 (BSA/Au-4). The SAXS curves were fitted by SASREF under these conditions (Fig. 7). It was found that the native BSA structure is slightly altered and the protein adopts a more open structure (Fig. 8). Adjusting the pH to 7 (BSA/Au-7) the opening is more pronounced. Further increasing the pH to 12 (BSA/Au-12) the protein loses its tertiary structure, however these SAXS data cannot be fitted by the Debye chain model either, which suggests secondary structure elements still present in the unfolded protein. Readjusting to neutral pH (BSA/Au-7Re), we obtain a scattering curve, which can again be fitted by SASREF. The fit suggests a more opened structure at the recovered pH = 7 than that of the initial neutral state before the pH cycle.

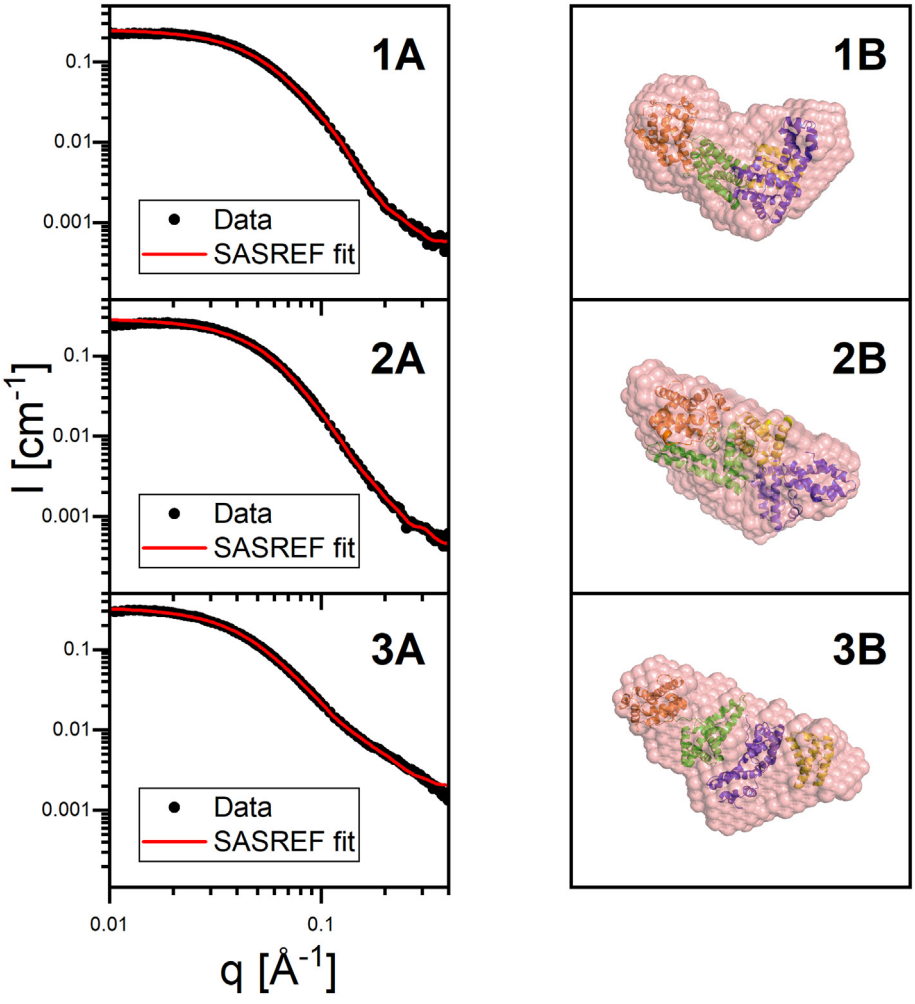


**Fig. 7.** Representative SAXS curves of BSA-$HAuCl_4$ bioconjugates fitted by SASREF. 1A: BSA/Au-4, 2A: BSA/Au-7, 3A: BSA/Au-7Re. 1B, 2B and 3B: the obtained BSA structures.

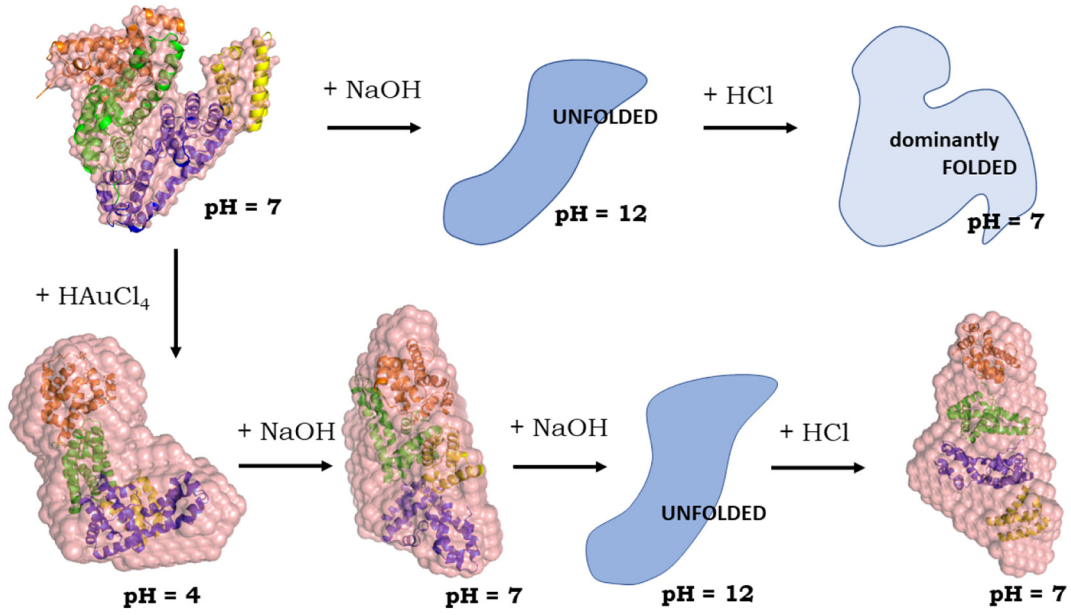


**Fig. 8.** Structure of BSA and BSA-$HAuCl_4$ systems in the function of pH.

## 4. Conclusion

The red-emitting fluorescence is the unique and most significant feature of BSA-Au bioconjugates. The performed experimental studies witnessed that the evolvement and change of this propriety is primarily related to the solution pH value dependent global conformational changes of BSA observed by SAXS, which is accompanied by significant structural changes at atomic level as revealed by IR spectroscopy. The conformation of BSA structure is not reversible after a neutral - alkali -neutral cycle, and its consequence can be observed in fluorescent spectra. The irreversibility of this cycle is more pronounced in presence of gold(III) ions. This is manifested in the largely enhanced red fluorescence intensity at pH = 7 after a neutral-alkali-neutral cycle (BSA/Au-7Re). The estimated ratios of secondary structure elements, together with the fitted global morphologies, indicate that each step of perturbation (change in pH value, thermal treatment, absence or presence of gold salt) may influence different domains of BSA whereby the global structure is altered. The experimental facts show that the complex protein structure is largely history dependent and its total recovery is hindered within the experimental time-range. The significant conformational changes of BSA, induced by gold salt, may play an important role in the evolution of the fluorescence behaviour of BSA-gold conjugates.

## Declaration of competing interest

The authors declare that they have no known competing financial interests or personal relationships that could have appeared to influence the work reported in this paper.

## Acknowledgments

This work was completed in the ELTE Thematic Excellence Programme (Synthesis+) supported by the Hungarian Ministry for Innovation and Technology as well as in the ELTE Institutional Excellence Programme supported by the National Research, Development and Innovation Office (NKFIH-1157-8/g2019-DT). Project no. 2018-1.2.1-NKP-2018-00005 has also been implemented with the support provided from the National Research, Development and Innovation Fund of Hungary, financed under the 2018-1.2.1-NKP funding scheme. This publication was produced under the operation program called Research and Innovation for the project: "Support of research and development capacities in the area of nanochemical and supramolecular systems", code ITMS2014+ 313011T583, funded from the resources of the European Regional Development Fund. Support from Independent Research Fund Denmark (Natural Sciences, grant no 4002-00479 and grant no 8021-00133B) and Independent Research Fund Denmark (Technology and Production, grant no 4184-00218) are gratefully acknowledged for funding.

## References

[1] H.-S. Peng, D.T. Chiu, Soft fluorescent nanomaterials for biological and biomedical imaging, Chem. Soc. Rev. 44 (14) (2015) 4699–4722, https://doi.org/10.1039/C4CS00294F.
[2] J. Xie, Y. Zheng, J.Y. Ying, Protein-directed synthesis of highly fluorescent gold nanoclusters, J. Am. Chem. Soc. 131 (3) (2009) 888–889, https://doi.org/10.1021/ja806804u.
[3] Y. Qiu, J. Huang, L. Jia, A turn-on fluorescent sensor for glutathione based on bovine serum albumin-stabilized gold nanoclusters, International Journal of Analytical Chemistry (2018) (2018) 1979684, https://doi.org/10.1155/2018/1979684.
[4] Y. Zhang, M. Wu, W. Dai, M. Chen, Z. Guo, X. Wang, D. Tan, K. Shi, L. Xue, S. Liu, Y. Lei, High drug-loading gold nanoclusters for responsive glucose control in type 1 diabetes, Journal of Nanobiotechnology 17 (1) (2019) 74, https://doi.org/10.1186/s12951-019-0505-z.
[5] P.J. Sadler, A. Tucker, pH-induced structural transitions of bovine serum albumin, Eur. J. Biochem. 212 (3) (1993) 811–817, https://doi.org/10.1111/j.1432-1033.1993.tb17722.x.
[6] X. Wen, P. Yu, Y.-R. Toh, J. Tang, Structure-correlated dual fluorescent bands in BSA-protected Au25 nanoclusters, J. Phys. Chem. C 116 (21) (2012) 11830–11836, https://doi.org/10.1021/jp303530h.
[7] H. Lin, K. Imakita, M. Fujii, C. Sun, B. Chen, T. Kanno, H. Sugimoto, New insights into the red luminescent bovine serum albumin conjugated gold nanospecies, J. Alloys Compd. 691 (2017) 860–865, https://doi.org/10.1016/j.jallcom.2016.08.300.
[8] J.M. Dixon, S. Egusa, Conformational change-induced fluorescence of bovine serum albumin–gold complexes, J. Am. Chem. Soc. 140 (6) (2018) 2265–2271, https://doi.org/10.1021/jacs.7b11712.
[9] X.-L. Cao, H.-W. Li, Y. Yue, Y. Wu, pH-induced conformational changes of BSA in fluorescent AuNCs@BSA and its effects on NCs emission, Vib. Spectrosc. 65 (2013) 186–192, https://doi.org/10.1016/j.vibspec.2013.01.004.
[10] A. Schwamberger, B. De Roo, D. Jacob, L. Dillemans, L. Bruegemann, J.W. Seo, J.P. Locquet, Combining SAXS and DLS for simultaneous measurements and time-resolved monitoring of nanoparticle synthesis, Nucl. Instrum. Methods Phys. Res., Sect. B 343 (2015) 116–122, https://doi.org/10.1016/j.nimb.2014.11.049.
[11] Y. Li, R. Beck, T. Huang, M.C. Choi, M. Divinagracia, Scatterless hybrid metal–single-crystal slit for small-angle X-ray scattering and high-resolution X-ray diffraction, J. Appl. Crystallogr. 41 (6) (2008) 1134–1139, https://doi.org/10.1107/S0021889808031129.
[12] E.M. Steiner, J. Lyngsø, J.E. Guy, G. Bourenkov, Y. Lindqvist, T.R. Schneider, J.S. Pedersen, G. Schneider, R. Schnell, The structure of the N-terminal module of the cell wall hydrolase RipA and its role in regulating catalytic activity, Proteins:

Structure, Function, and Bioinformatics 86 (9) (2018) 912–923, https://doi.org/10.1002/prot.25523.
[13] M.V. Petoukhov, D.I. Svergun, Global rigid body modeling of macromolecular complexes against small-angle scattering data, Biophys. J. 89 (2) (2005) 1237–1250, https://doi.org/10.1529/biophysj.105.064154.
[14] A. Bujacz, Structures of bovine, equine and leporine serum albumin, Acta Crystallogr. D Biol. Crystallogr. 68 (10) (2012) 1278–1289, https://doi.org/10.1107/S0907444912027047.
[15] V.V. Volkov, D.I. Svergun, Uniqueness of ab initio shape determination in small-angle scattering, J. Appl. Crystallogr. 36 (3–1) (2003) 860–864, https://doi.org/10.1107/S0021889803000268.
[16] A. Barth, C. Zscherp, What vibrations tell about proteins, Q. Rev. Biophys. 35 (4) (2002) 369–430, https://doi.org/10.1017/S0033583502003815.
[17] A. Barth, Infrared spectroscopy of proteins, Biochimica et Biophysica Acta (BBA) - Bioenergetics 1767 (9) (2007) 1073–1101, https://doi.org/10.1016/j.bbabio.2007.06.004.
[18] K.P. Ishida, P.R. Griffiths, Comparison of the amide I/II intensity ratio of solution and solid-state proteins sampled by transmission, attenuated total reflectance, and diffuse reflectance spectrometry, Appl. Spectrosc. 47 (1993) 584–589, https://doi.org/10.1366/0003702934067306.
[19] R. Lu, W.-W. Li, A. Katzir, Y. Raichlin, H.-Q. Yu, B. Mizaikoff, Probing the secondary structure of bovine serum albumin during heat-induced denaturation using mid-infrared fiberoptic sensors, Analyst 140 (3) (2015) 765–770, https://doi.org/10.1039/C4AN01495B.
[20] K. Solti, W.-L. Kuan, B. Fórizs, G. Kustos, J. Mihály, Z. Varga, B. Herberth, É. Moravcsik, R. Kiss, M. Kárpáti, A. Mikes, Y. Zhao, T. Imre, J.-C. Rochet, F. Aigbirhio, C.H. Williams-Gray, R.A. Barker, G. Tóth, DJ-1 can form $\beta$-sheet structured aggregates that co-localize with pathological amyloid deposits, Neurobiol. Dis. 134 (2020) 104629, https://doi.org/10.1016/j.nbd.2019.104629.
[21] P. Debye, Molecular-weight determination by light scattering, The Journal of Physical and Colloid Chemistry 51 (1) (1947) 18–32, https://doi.org/10.1021/j150451a002.